Eggenhuisen, T.M., Munnik, P., Talsma, H., de Jongh, P.E. and de Jong, K.P., *Journal of Catalysis 297 (2013), 306-313.*
DOI: 10.1016/j.jcat.2012.10.024

Freeze-Drying for Controlled Nanoparticle Distribution in Co/SiO_2 Fischer-Tropsch Catalysts

T.M. Eggenhuisen[*,a], P. Munnik[*,a], H. Talsma[b], P.E. de Jongh[a] and K.P. de Jong[#,a]

[a] Inorganic Chemistry and Catalysis, Debye Institute for Nanomaterials Science, Utrecht University, Universiteitsweg 99, 3584 CG Utrecht, The Netherlands
[b] Pharmaceutics, Utrecht Institute for Pharmaceutical Science, Utrecht University, Universiteitsweg 99, 3584 CG Utrecht, The Netherlands

[*]Both authors contributed equally to this work
[#] Corresponding author email: k.p.dejong@uu.nl, phone: +31 30 253 7400, fax: +31 30 251 1027

Research highlights

- Cobalt nanoparticle distribution on a commercial silica-gel was manipulated
- Freeze-drying parameters were established using differential scanning calorimetry
- Conventional drying led to 10 – 400 nm clusters of 6 – 8 nm Co_3O_4 nanoparticles
- Uniformly distributed 4 – 7 nm nanoparticles were obtained by freeze-drying
- Model systems synthesized for deactivation studies for the Fischer-Tropsch reaction

Graphical abstract

Freeze-drying was successfully applied to control the nanoparticle distribution in Co/SiO_2 Fischer-Tropsch catalysts with 4 to 8 nm Co_3O_4 nanoparticles prepared from a cobalt nitrate precursor. As-synthesized catalysts with clusters, uniformly distributed nanoparticles or an egg-shell configuration on a silica-gel support form a platform to study the effect of nanoparticle spacing on deactivation.

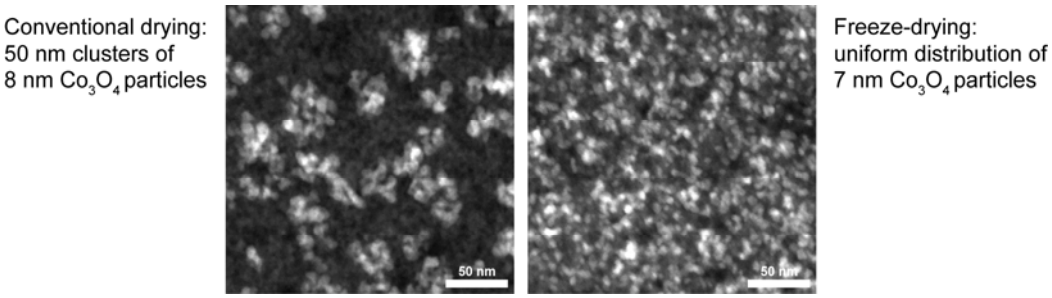

Abstract

Controlling the nanoparticle distribution over a support is considered essential to arrive at more stable catalysts. By developing a novel freeze drying method, the nanoparticle distribution was successfully manipulated for the preparation of Co/SiO_2 Fischer-Tropsch catalysts using a commercial silica-gel support. After loading the precursor via a solution impregnation or melt infiltration, differential scanning calorimetry was used to study the phase behavior of the confined cobalt nitrate precursor phases to ascertain suitable freeze-drying conditions. When a conventional drying treatment was utilized, catalysts showed inhomogeneous cobalt distributions, with 6 – 8 nm nanoparticles grouped in clusters of up to 400 nm. In contrast, by utilizing freeze-drying starting at liquid nitrogen temperatures, homogeneous distributions of 4 – 7 nm nanoparticles were obtained. Raising the temperature at which the freeze drying process takes place resulted in either uniform or strongly non-uniform nanoparticle distributions, depending on the specific conditions and precursor loading method. After reduction, all catalysts showed high activity for the Fischer-Tropsch reaction at 1 bar. The catalysts thus synthesized form an excellent platform for future studies of the stability under industrially relevant Fischer-Tropsch conditions.

Keywords: nanoparticle synthesis, lyophilization, freeze-drying, supported catalysts, catalyst preparation, Fischer-Tropsch synthesis, cobalt, deactivation, sintering, transition metal nitrates

1. Introduction

Coalescence and sintering of nanoparticles is an irreversible deactivation pathway with detrimental effects on the activity and life time of supported catalysts [1, 2]. Therefore, many innovative pathways have been developed to improve stability of heterogeneous catalysts, such as encapsulation by a metal oxide shell around colloidal nanoparticles [3, 4] or by a porous metal oxide layer covering supported nanoparticles [5], and restriction of nanoparticle mobility by using cagelike support materials [6] or by alloying with a metal with a higher melting point [7]. Nevertheless, for supported nanoparticles maximizing nearest neighbor distances or, in other words, achieving a uniform nanoparticle distribution is essential to improve catalytic stability. Indeed, non-uniform nanoparticle distributions have been observed in many metal-support systems and showed to be prone to sintering [8, 9]. On the other hand, a non-uniform distribution of the active phase over microns or even millimeters in macroscopic catalyst bodies may be preferred depending on the catalysis conditions [10]. For example, deposition of the active phase in the outer rim of a macroscopic support body, a so-called egg-shell configuration, is favorable for fast reactions combined with diffusion constrictions of substrates and products [11]. Therefore, active control over metal or metal oxide nanoparticle distribution on a support on different lengths scales is crucial to the rational synthesis of supported catalysts.

Impregnation and drying is a convenient catalyst preparation method and is commonly applied in industry and academia. With the use of highly soluble transition metal nitrate salts, waste streams are low and high metal loadings can be obtained in a single impregnation step. Nevertheless, controlling dispersion and distribution by this synthesis route has remained challenging [12-15]. Especially at high metal loadings [16] and low support-salt interactions [17], agglomeration and cluster formation of nanoparticles after calcination is difficult to prevent. Drying has been recognized as a

major influence on the distribution of the active phase over macroscopic bodies [18-20]. And although alternatives have been developed [21-24], a method preserving the advantages of impregnation and drying is desirable. Here, we will explore in detail the potential of freeze-drying for controlled nanoparticle distribution on an industrially relevant silica-gel support for the preparation of Co/SiO_2 Fischer-Tropsch catalysts.

Freeze-drying is a drying method often encountered in food-processing [25, 26] as well as in the pharmaceutical industry [27-29] usually for preservation purposes. By freeze-drying a solvent can be removed without exposing the matrix to tensile forces of a receding meniscus. Therefore, it is a suitable drying technique for the cryo-preservation of biological tissues [30, 31] or to develop porous aerogels based on soft templates from polymeric materials [32, 33]. For catalyst preparation, freeze-drying has been suggested to reduce precursor solution mobility during drying and therefore control the location of deposition of the precursor phase. Nevertheless, few applications have been reported [34-37].

Freeze-drying generally consists of three steps: freezing, primary drying and secondary drying [38, 39]. Freeze-drying processes for complex solutions most often result from experimentally based considerations and seems an art rather than a science [40]. Freezing is actually the most important step, as it determines the ice crystalline structure, which is affected by the cooling rate, degree of supercooling and annealing [41-43]. During primary drying, ice sublimates due to the reduced pressure. The rate depends on the heat transfer determined mainly by the ice structure, pressure and temperature [44]. However, several experimental details have a large influence on this step, even the sample vial configuration [45]. Finally, non-freezing or amorphous water can be removed in the secondary drying step, during which the temperature is raised under reduced pressure [46].

Due to its long history and industrial relevance, literature on freeze-drying of (bio)pharmaceutical formulations and food is extensive. Here we aim to obtain the first fundamental insight into freeze-drying for the preparation of Co/SiO_2 Fischer-Tropsch catalysts. To develop a suitable freeze-drying method, The phase behavior of $Co(NO_3)_2$ (aq) solution and $Co(NO_3)_2{\cdot}6H_2O$ salt confined within a mesoporous silica matrix was studied with DSC. The phases present after freeze-drying were identified and compared to those resulting from conventional drying treatments. Detailed assessment of the distribution of the cobalt oxide nanoparticles after decomposition of the nitrates was done using ultramicrotomy and TEM. The fundamental insights on precursor phase behavior combined with freeze-drying led to control over the nanoparticle distribution on an industrially relevant silica gel support. Thus a platform was created for future investigation of the effect of uniform, clustered or egg-shell configurations on catalyst stability.

2. Materials and Methods

2.1 Catalyst Synthesis

Co/SiO_2 catalysts were prepared using a commercially available silica gel as support (Davicat 1404, Grace-Davidson). The support was sieved to a fraction of 38 - 75 μm and the porous properties were characterized with N_2-physisorption at -196 ºC (Tristar 3000, Micromeritics): V_p = 0.87 cm^3/g, S_{BET} = 443 m^2/g, d_p = 8 nm. Solution impregnation (SI) was performed to incipient wetness using a saturated $Co(NO_3)_2$ (aq) solution (4.2 M, $Co(NO_3)_2{\cdot}6H_2O$, >99% Sigma-Aldrich), leading to a nominal cobalt metal loading of 17 wt%. For melt infiltration (MI), for example, 929 mg of $Co(NO_3)_2{\cdot}6H_2O$ and 754 mg of SiO_2-gel were physically mixed in a mortar with a

pestle. The physical mixture was then heated overnight at 60 ºC in a Teflon-lined steel autoclave (~6 mL). A nominal cobalt metal loading of 20 wt% was obtained.

Different drying treatments were applied to the as-prepared SiO_2-SI and SiO_2-MI precursor loaded catalysts. Conventional drying (CD) for SiO_2-SI was performed in a crucible in a preheated muffle oven at 60 ºC overnight, after which the sample was handled under ambient conditions. Melt infiltrated samples were used as-prepared. Freeze-drying (FD) was performed using a Sublimator 400 Freeze-dryer (Zirbus) and using the conditions summarized in Table 1. Samples were freeze-dried in 2 mL glass vials. The two freeze-drying procedures are denoted by their freezing temperature and the shelf temperature during the primary drying step. In the method FD(-45/-30), samples were frozen on the shelf by cooling to -45 ºC (~1 ºC/min, 5 hours). Primary drying was started by reducing the chamber pressure, after which the shelf temperature was increased to -30 ºC. For FD(LN_2/-45), quench freezing with liquid N_2 was applied. The glass vials containing the samples were cooled down in a reservoir containing liquid nitrogen, after which the reservoir was placed on the precooled shelf at -45 ºC in the freeze-dryer. Subsequently, the chamber pressure was reduced to start the primary drying step. Both methods included secondary drying by step-wise heating to 20 ºC under reduced pressure. The condenser temperature was between -65 and -70 ºC and the condenser chamber pressure was 0.02-0.03 mbar.

Table 1
Summary of freeze-drying conditions.

	FD(-45/-30)	FD(LN_2/-45)
freezing temperature (time)	-45 ºC (5 h)	~ -170 ºC (15 min)
shelf temperature primary drying (time)	-30 ºC (82 h)	-45 ºC (48 h)
primary drying pressure	0.02-0.03 mbar	0.02-0.03 mbar
shelf temperature secondary drying (time)	-10 ºC (3 h), 20 ºC	-30 ºC (12 h), -15 ºC (12 h), 20 ºC
secondary drying pressure	<0.02 mbar	<0.02 mbar

Calcination of all precursor loaded catalysts was performed by heating to 350 ºC (1 ºC/min, 1 hour) in a flow of N_2 or 1% v/v NO/N_2 (100 mL/min/100 mg catalyst). Freeze-dried pre-catalysts were transferred under dry nitrogen atmosphere to a fluidized-bed reactor.

2.2 Catalyst Characterization

The phase behavior of cobalt nitrate present during the different stages of catalyst preparation was analyzed using differential scanning calorimetry (DSC, Q2000, TA Instruments). The temperature and heat flow were calibrated with a certified indium sample and measurements were performed with hermetically sealed aluminum pans (~40 µL, Tzero, TA Instruments) under a flow of N_2 (50 mL/min). Sample masses were typically between 5 - 15 mg and heat flows were recorded between -90 ºC and 75 ºC at a rate of 1 ºC/min.

Thermogravimetric analysis (TGA, Q50 TA Instruments) was used to determine the residual water after different drying treatments by measuring the weight loss after heating to 500 ºC for 30 min, at a heating rate 10 ºC/min and an N_2 flow of 60 mL/min. The weight loss was corrected for the loss of water by condensation of silanol groups from the pristine silica gel, which was experimentally found to occur between 150 ºC and 500 ºC. Thus, the rest of the weight loss could be attributed to the

loss of any residual water and the decomposition of Co(NO3)2 to Co_3O_4. The amount of residual water was calculated in moles H_2O/mole Co from the resulting corrected weight loss (m_{loss}).

Diffuse Reflectance Spectroscopy (DRS) was used to obtain the UV/VIS absorption spectra of dried samples. Measurements were obtained on a Varian Cary 500 spectrophotometer from 800 to 250 nm in diffuse reflectance mode. Samples were held in an air tight sample holder with a quartz window to prevent rehydration during measurements.

XRD patterns were recorded between 30 and 60 º2θ with a Bruker-AXS D2 Phaser X-ray Diffractometer using Co-$K_{\alpha 12}$ radiation (λ = 1.790 Å). The volume averaged Co_3O_4 crystallite size was determined using the Scherrer equation with a shape factor k = 0.9 and line broadening analysis on the (110), (111) and (200) peaks by a fitting procedure in Eva2 software (Bruker AXS).

The catalyst particles after calcination were embedded in a two component epoxy resin (Epofix, EMS) and cured at 60 °C overnight. The embedded catalysts were then cut into thin sections with a nominal thickness of 50 nm using a Diatome Ultra 35° diamond knife mounted on a Reichert-Jung Ultracut E microtome and collected on a TEM grid. Bright field TEM images were obtained on a Tecnai 12, operated at 120 keV. High angle annular dark field (HAAFD) STEM was performed on a Tecnai 20 equipped with a field emission gun and operated at 200 keV.

2.3 Catalytic Testing

Fischer-Tropsch synthesis was performed at 220 ºC and 1 bar with a H_2/CO ratio of 2 v/v. Typically, a plug-flow reactor was loaded with 10 mg of catalyst diluted with 200 mg SiC (200 μm). The catalysts were reduced *in-situ* at 500 ºC for 2 hrs (heating rate 5 ºC/min) under a flow or H_2/Ar (20/40 mL/min). C_1-C_{15} products were analyzed by online gas chromatography (Varian 430 GC, CP sil-5). The catalytic activity, expressed as cobalt-time-yield (10^{-5} $mol_{CO}/g_{Co}/s$) and C_1/C_{5+} selectivity, expressed in wt%, were determined after 20 hrs reaction time and a CO conversion of 2%.

3. Results & Discussion

3.1 Freeze-Drying Methods for Confined $Co(NO_3)_2$ (aq) and $Co(NO_3)_2 \cdot 6H_2O$

To develop suitable freeze-drying methods, the phase behavior of cobalt nitrate confined in the mesoporous silica gel support was studied with differential scanning calorimetry (DSC). Fig. 1 shows the freezing and melting behavior observed for silica gel after solution impregnation (SI) with $Co(NO_3)_3$ (aq) and after melt infiltration (MI) with $Co(NO_3)_2 \cdot 6H_2O$. Different freezing and melting point depressions were observed for the confined cobalt nitrate solution and for the cobalt nitrate salt. For SiO_2-MI, a single freezing and a single melting event were detected, indicating a uniform composition and structure of the confined salt. Bulk $Co(NO_3)_2 \cdot 6H_2O$ melts at 55 ºC, therefore, the confinement in the silica matrix caused a melting point depression of 35 ºC. The solution impregnated on silica gel displayed more complex phase behavior with several crystallization and melting events. A saturated aqueous $Co(NO_3)_2$ solution melts at -31 ºC. Therefore, the broad melting peak with a maximum at -35 ºC was ascribed to residual extraporous solution. The melting peak with maximum at -54 ºC was tentatively attributed to the confined solution, which would correspond to a melting point depression of 23 ºC. The melting peak at 10 ºC as well as the freezing peak at -30 ºC were tentatively ascribed to

melting and freezing of confined $Co(NO_3)_2 \cdot 6H_2O$, indicating that some phase separation of the solution occurred inside the pore system. The amount of water present in the sample has a huge impact on the absolute freezing and melting point; comparing SI and MI shows a 55 ºC difference which will be important for subsequent drying treatments.

Two freeze-drying conditions can be deduced from the DSC thermograms. Firstly, the closed arrows in Fig. 1 indicate the minimum freezing temperature to solidify all cobalt nitrate. For SiO_2-SI, exotherm peaks are observed at -62 ºC and -75 ºC indicating that a freezing temperature of at least -85 ºC is needed, while for SiO_2-MI -30 ºC would suffice as freezing temperature. Second, the sample temperature during drying should not exceed the onset at which the precursor begins to melt. Therefore, as indicated by the open arrows, freeze-drying conditions should be chosen such that SiO_2-SI remains below -65 ºC and SiO_2-MI below -10 ºC.

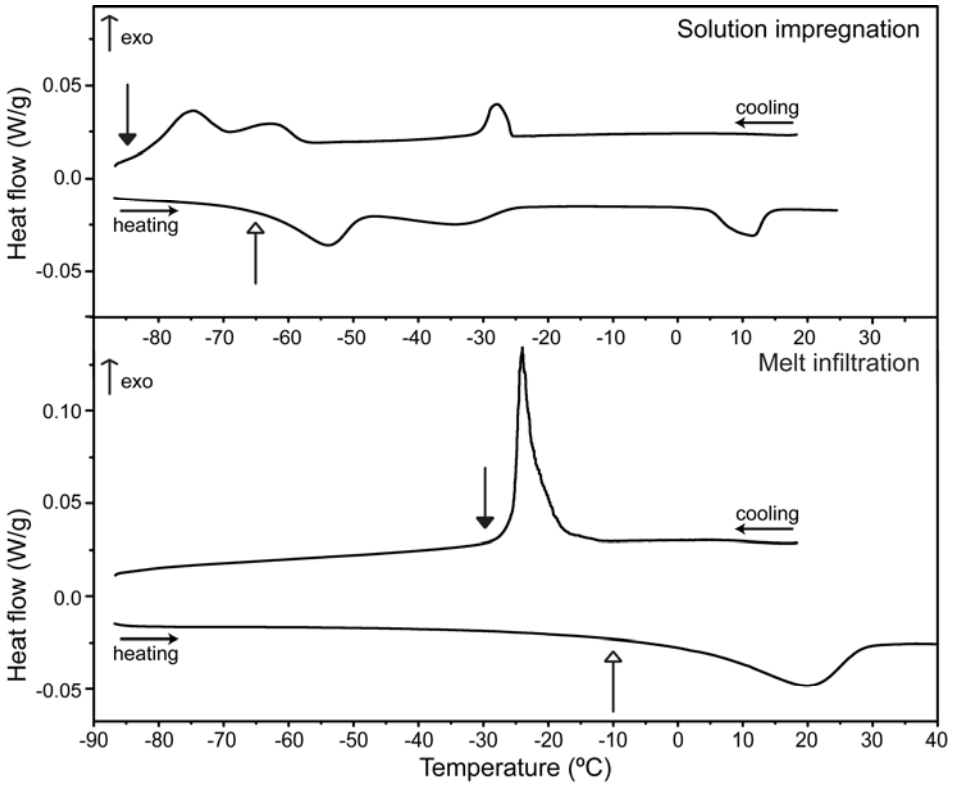

Fig. 1. DSC thermograms recorded for precursor loaded silica gel prepared via solution impregnation (SI) with $Co(NO_3)_2$ (aq) or melt infiltration (MI) with $Co(NO_3)_2 \cdot 6H_2O$. Closed arrows indicate minimum freezing temperature and open arrows indicate maximum sample temperature during freeze-drying. Cooling/heating rate 1 ºC/min, thermograms are offset for clarity.

Based on the results from DSC, two freeze-drying methods were developed within the boundaries set by experimental equipment. The first method, denoted by FD(LN_2/-45) involved quench freezing by liquid nitrogen, which should solidify both the confined cobalt nitrate solution (SI) as well as the salt (MI). Samples were then placed on a precooled shelf at -45 ºC for the primary drying step. In the second freeze-drying method, FD(-45/-30) a higher freezing temperature (-45 ºC) and a higher shelf temperature during primary drying (-30 ºC) were applied. By this method, the confined cobalt nitrate solution will not freeze, but the cobalt nitrate salt will. In both methods, the pressure range during primary drying was 0.02-0.03 mbar, which

corresponds to an ice (I_h) equilibrium temperature of -55 ºC to -53 ºC. This temperature is low enough during primary drying in both methods to keep SiO_2-MI frozen. However, for SiO_2-SI the DSC data suggests this temperature is too high, and thus this sample will only remain frozen in FD(LN_2/-45) by self-cooling at sufficiently high freeze-drying rates. While it was not possible to measure the actual drying rate, an indirect indication is the resulting cobalt distribution over the support. A homogeneous distribution will indicate the drying rate was sufficiently high to keep the sample frozen, while an inhomogeneous distribution will indicate mobility of the precursor. In both methods, the heat for sublimation is provided by the shelf temperature, while the actual sample temperature is dependent on the rate of freeze-drying, the structure of the ice, the chamber pressure and the condenser temperature (see Table 1 for experimental details). Thus, the mobility of the precursor phase is expected to be restricted by FD(LN_2/-45) for both SiO_2-SI and SiO_2-MI. With FD(-45/-30), precursor immobilization is expected for SiO_2-MI, while for SiO_2-SI mobility of the solution is likely.

3.2 Cobalt Nitrate Precursor Phase after Drying

by TGA, DSC and UV/VIS and the results are summarized in Table 2. The conventional drying was performed in a muffle oven to simulate the static nature of the freeze dryer. The drying was performed at 60 °C to prevent preliminary decomposition of the precursor. The residual water was quantified using TGA analysis. After conventional drying, 6.5 and 7.8 moles of H_2O per mole of cobalt remained for SI and MI respectively. The samples were handled under ambient air conditions, and therefore rehydration of the salt could have occurred. Indeed, for SI-CD a sample transferred directly from the muffle oven at 60 ºC to the drybox contained only 4.9 residual water molecules per mole of Co. Thus, some re-adsorption had occurred due to the hydrophilic nature of cobalt nitrate. However, this did not affect the final metal distributions as was observed with TEM. After melt infiltration, the water to cobalt ratio was slightly higher than for the $Co(NO_3)_2 \cdot 6H_2O$ from stock. This is partly due to the presence of physisorbed water in the silica gel, as the support was not dried prior to melt infiltration. After both freeze-drying treatments, water contents between 0.1 and 0.9 H_2O/Co were found for SI and MI. The different hydration states of cobalt nitrate depended on the drying method. This was also clearly observed in the derivative weight change profiles during decomposition, as shown in Fig. 2. For Si-CD, decomposition occurred largely in two steps: dehydration and decomposition of the nitrate which corresponds to results reported earlier [47]. For the samples obtained after freeze-drying, dehydration was virtually absent and decomposition occurred in a single step.

Table 2
Hydration state of precursor loaded silica gel prepared via solution impregnation (SI) with $Co(NO_3)_2$ (aq) and melt infiltration (MI) with $Co(NO_3)_2 \cdot 6H_2O$ after conventional drying (CD) or freeze-drying (FD).

Precursor loading	Drying method	Residual water (moles H_2O /mole Co)[a]	DSC melting peak maximum (ºC)[b]	UV-VIS absorption maximum (nm)
SI	CD	6.5	19	514
SI	FD(-45/-30)	0.1	none	540
SI	FD(LN_2/-45)	0.7	none	538
MI	none	7.8	20	510
MI	FD(-45/-30)	0.9	none	539
MI	FD(LN_2/-45)	0.7	none	542

[a] determined by TGA, [b] maximum of melting point

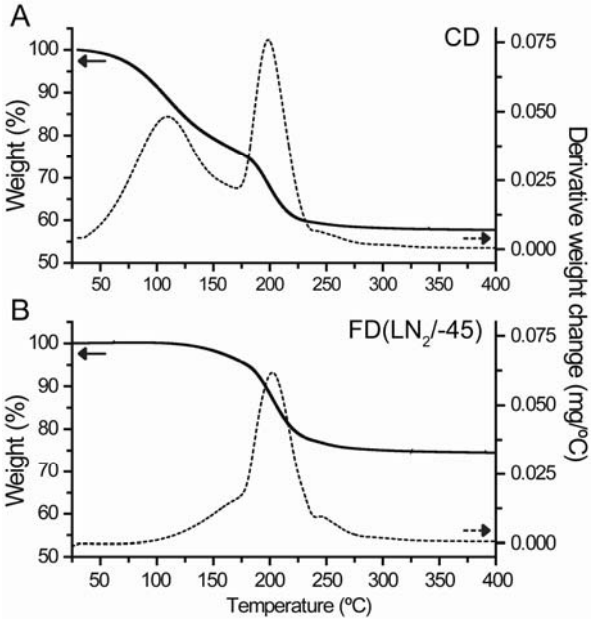

Fig. 2. Weight loss determined with TGA (5 ºC/min) for precursor loaded silica gel prepared via solution impregnation (SI) with $Co(NO_3)_2$ (aq) (A) after conventional drying at 60 ºC (CD) and (B) after freeze-drying (FD(LN_2/-45)).

Further information on the precursor phase after drying was deduced from the phase behavior observed with DSC. Fig. 3 shows the melting behavior of the precursor loaded silica gel after the different drying treatments. SI-CD and MI showed a single melting peak at 20 ºC, which has been ascribed to confined cobalt nitrate hexahydrate before [48]. Thus, both SI-CD and MI resulted in confined, liquid cobalt nitrate hexahydrate salt at room temperature. No melting transitions were observed after freeze-drying. The hydration state was also studied by UV/VIS spectroscopy, as after conventional drying both SI and MI samples were pink, while after freeze-drying they had turned purple. Indeed, the main UV/VIS absorption band shifted from 510 nm, which corresponds to octahedral cobalt nitrate hexahydrate, to 540 nm for freeze-dried samples (Table 2). This suggests exchange of H_2O ligands for NO_3^- or a surface

hydroxyl group, which both have a smaller ligand-field splitting parameter and therefore cause a shift of the absorption to lower energy [49].

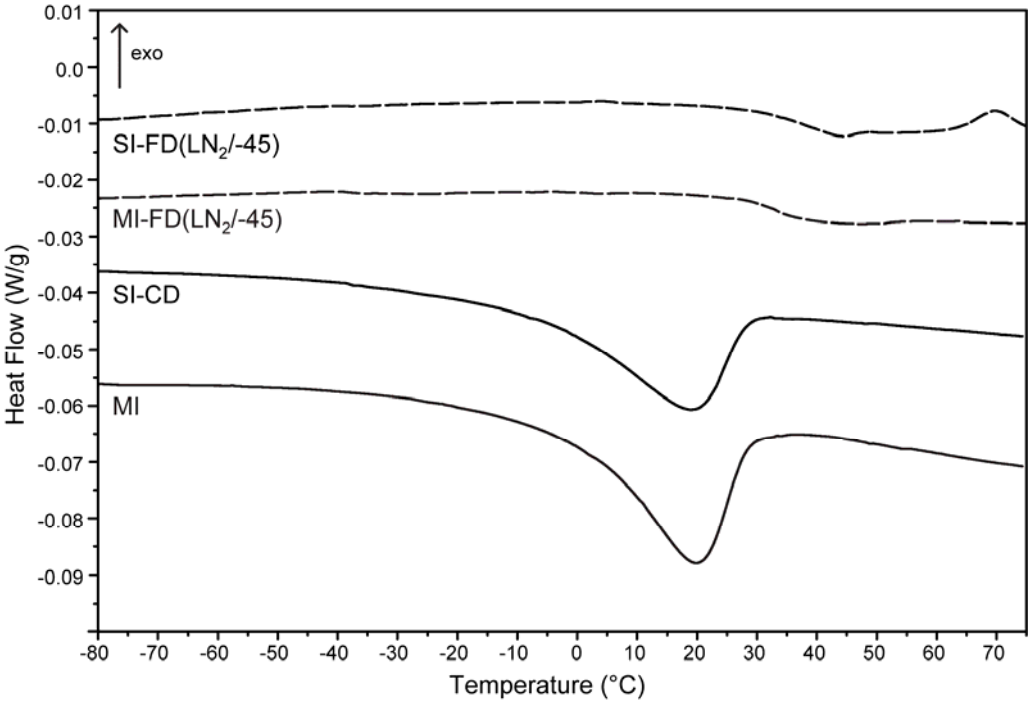

Fig. 3. DSC thermograms (heating rate 1 ºC/min) recorded for precursor loaded silica gel prepared via solution impregnation (SI) with $Co(NO_3)_2$ (aq) and melt infiltration (MI) with $Co(NO_3)_2 \cdot 6H_2O$ after conventional drying at 60 ºC (CD) and after freeze-drying (FD(LN_2/-45)).

3.3 Effect of Drying on Co_3O_4 Distribution at the Micrometer Length Scale

The effect of the precursor distribution on the cobalt oxide distribution after calcination was imaged. Preparation of ~50 nm thick slices by ultramicrotomy allowed detailed TEM analysis of nanoparticle size and distribution over the support. First, the distribution of Co_3O_4 over the silica gel particle on the micrometer scale will be discussed, while the next section addresses the dispersion and distribution of individual Co_3O_4 nanoparticles on the nanometer scale.

Fig. 4 shows micrographs recorded for catalysts prepared by different drying treatments followed by calcination in a flow of N_2. In most cases clusters were observed with sizes ranging from 10 to 40 nm. Please note that the clusters appeared to consist of a (large) number of individual nanoparticles of about 8 nm in size (*vide infra*). Three types of cobalt oxide distribution over the support particles were identified. After conventional treatment of both SI and MI (Fig. 4A and D), ~40 nm clusters were distributed homogeneously over the whole support. Second, freeze-drying by liquid nitrogen freezing (Fig. 4C and F) as well as FD(-45/-30) for MI (Fig. 4E) led to a homogeneous distribution of very small Co_3O_4 clusters below 20 nm. Last, by solution impregnation and FD(-45/-30) shown in Fig. 4B, clusters up to 140 nm were observed. Surprisingly, an egg-shell configuration was apparent for this catalyst at lower magnification and cobalt clusters were only observed in the ~5 μm outer rim, while the body of the particle was mostly empty (Fig. 5). Thus, FD(-45/-30) caused extensive redistribution of the cobalt nitrate solution to the surface of the macroscopic support particle, while for the sample melt infiltrated with

$Co(NO_3)_2 \cdot 6H_2O$ this drying method led to a homogeneous distribution after calcination.

The different distributions are attributed to the mobility of the precursor and the rate of drying. During conventional drying at 60 °C, the precursor is liquid (either in solute state or molten) allowing for mobility and redistribution, resulting in an inhomogeneous distribution. However, the drying rate at this temperature will be relatively high, limiting the timespan in which redistribution occurs and causing limited agglomeration. For SI-FD(-45/-30), a similar principle holds: if the precursor is not frozen mobility is expected. However, the drying rate will be relatively low due to the low vapour pressure, and redistribution can occur over a substantially longer period of time. We tentatively propose that due to the low support-precursor interactions and low drying rate, the precursor moved towards a drying front at the particle surface, resulting in an egg-shell distribution. For SI-FD(LN_2/-45), a homogeneous distribution is observed throughout the particle. This confirms that the precursor was completely immobilized during freezing, and that the drying rate was sufficiently high to keep the precursor frozen. The MI samples respond in a similar way to the drying procedures. However, the infiltrated cobalt nitrate hexahydrate of the MI samples has a higher freezing and melting point than the SI samples. Therefore, in the case of MI-FD(-45/-30) a temperature of -45 ºC was enough to solidify and thereby immobilize the precursor, preventing redistribution.

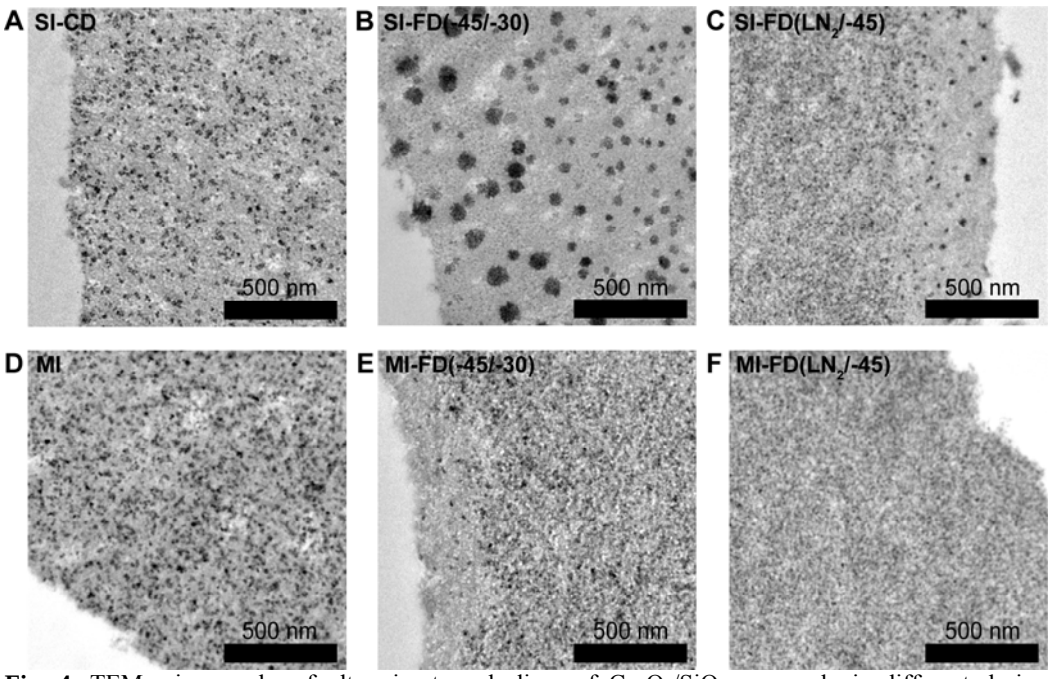

Fig. 4. TEM micrographs of ultramicrotomed slices of Co_3O_4/SiO_2 prepared via different drying treatments followed by calcination in a flow of N_2 prepared via solution impregnation (SI, top row) or melt infiltration (MI, bottom row) and conventional drying (left column, CD), freeze-drying (middle column, FD(-45/-30)) and freeze-drying (right column, FD(LN_2/-45)).

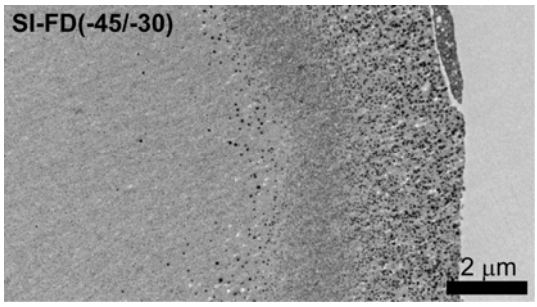

Fig. 5. TEM micrograph of ultramicrotomed slice of Co_3O_4/SiO_2 prepared via solution impregnation (SI) and freeze-drying (FD(-45/-30)) followed by calcination in a flow of N_2.

By calcination in a flow of N_2, mobility of cobalt during decomposition is expected [50]. By the addition of 1% v/v NO during calcination, aggregation is mostly prevented during decomposition of hydrated transition metal nitrates [13, 51]. Here NO calcination was applied to confirm the footprint of the salt distribution obtained after different drying treatments. TEM showed that the Co_3O_4 cluster distribution followed the same general trend as was observed after calcination in N_2 flow. Both SI and MI resulted in similar cobalt oxide cluster distributions after conventional drying or very homogeneous distributions after freeze-drying starting at liquid nitrogen temperatures. By FD(-45/-30), solution impregnation again led to an egg-shell configuration, while melt infiltration resulted in a homogeneous distribution. This similarity shows that the cobalt distribution on the micrometer length scale was mainly determined by the precursor phase distribution after drying. Only the cluster sizes after conventional drying differ; Fig. 6A shows clusters obtained after NO calcination can be substantially larger compared to those obtained after calcination in an N_2 flow, however this is in line with previous results.[52, 53] Regardless, it is clear that after conventional drying the cobalt distribution is very inhomogeneous. In contrast, freeze-drying starting at liquid nitrogen temperatures (Fig. 6B) again led to a homogeneous distribution of cobalt oxide.

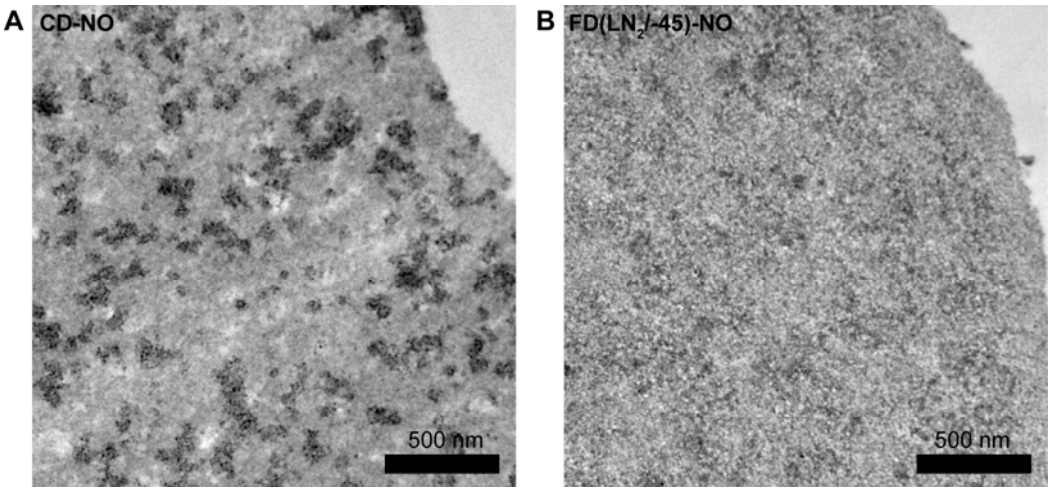

Fig. 6. TEM micrographs of ultramicrotomed slices of Co_3O_4/SiO_2 prepared via solution impregnation (SI) and different drying treatments followed by calcination in a flow of 1% NO/N_2: (A) conventional drying (CD) or (B) freeze-drying (FD(LN_2/-45)).

3.4 Effect of Drying on Co_3O_4 Nanoparticle Distribution at Nanometer Scale

Table 3 shows the results for average crystallite size as determined by XRD and average particle size from analysis of high angle annular dark field (HAADF) STEM images. After calcination in a flow of N_2, SI-CD led to the formation of 10-40 nm large clusters as can be seen in Fig. 7A. However, the clusters appeared to consist 8 nm nanoparticles, which corresponded to the average crystallite size from XRD. After calcination in 1% NO/N_2, larger clusters up to 400 nm were formed by SI-CD (Fig. 6A). However, in Fig. 7C it is clear that the large clusters consisted of ~6 nm individual nanoparticles. By freeze-drying (Fig. 7B and D), nanoparticles were found distributed uniformly over the support. Furthermore, by both calcination methods smaller Co_3O_4 nanoparticles formed after freeze-drying, i.e. ~7 nm by N_2 calcination and ~4 nm by NO calcination.

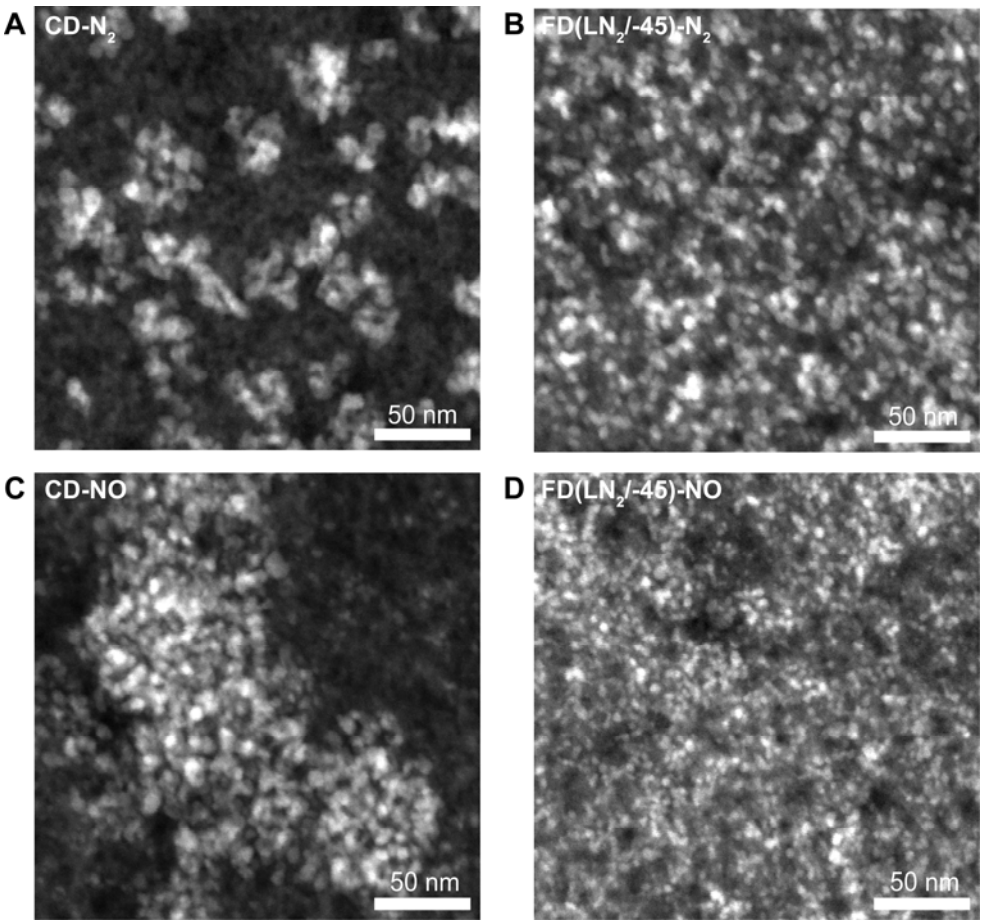

Fig. 7. HAADF-STEM micrographs of ultramicrotomed slices of Co_3O_4/SiO_2 prepared via solution impregnation (SI) and conventional drying (left column) or freeze-drying (right column) followed by calcination in a flow of N_2 (top row) or a flow of 1% NO/N_2 (bottom row): (A) CD-N_2, (B) FD(LN_2/-45)-N_2, (C) CD-NO, (D) FD(LN_2/-45)-NO.

Table 3
Average crystallite size determined with XRD and average particle size determined with HAADF STEM for catalysts after calcination in a flow of N_2 or a flow of 1% NO/N_2, prepared via solution impregnation (SI) with $Co(NO_3)_2$ (aq) and melt infiltration (MI) with $Co(NO_3)_2 \cdot 6H_2O$ and conventional drying at 60 ºC (CD) or after freeze-drying (FD).

Catalyst	Calcination in flow of N_2		Calcination in flow of 1% NO/N_2	
	d_{XRD} (nm)	d_{TEM} (nm)	d_{XRD} (nm)	d_{TEM} (nm)
Co_3O_4/SiO_2-SI-CD	8.0	7.9 ± 1.9	5.4	6.4 ± 1.7
Co_3O_4/SiO_2-SI-FD(-45/-30)	7.9	7.4 ± 1.8	4.7	5.5 ± 1.5
Co_3O_4/SiO_2-SI-FD(LN_2/-45)	7.8	6.6 ± 1.5	4.4	4.2 ± 0.8
Co_3O_4/SiO_2-MI	7.9	6.8 ± 1.5	6.2	6.0 ± 1.3
Co_3O_4/SiO_2-MI-FD(-45/-30)	7.9	7.3 ± 1.5	6.0	5.0 ± 1.1
Co_3O_4/SiO_2-MI-FD(LN_2/-45)	7.9	6.8 ± 1.4	4.2	4.6 ± 1.1

3.5 Co/SiO_2 Catalysts for the Fischer-Tropsch Synthesis

The Co_3O_4/SiO_2 catalysts prepared by different drying methods were tested for the Fischer-Tropsch synthesis. Table 4 shows the results of the catalytic tests at 1 bar and 2% conversion. The catalysts prepared by calcination in N_2 were activated by reduction at 450 ºC. The smaller particles obtained after calcination in NO/N_2 were reduced at 550 ºC, as these are more difficult to reduce than larger particles [54, 55]. They showed catalytic activities comparable to earlier reported highly active catalysts treated at the same reduction temperature[55]. The N_2 calcined catalysts exhibited a slightly lower Fischer-Tropsch activity, which is ascribed to the larger Co_3O_4 nanoparticle size [56]. The freeze-dried catalysts showed slightly higher activity as compared to the catalysts prepared by conventional drying. This indicates that the cobalt oxides formed after calcination and different drying treatments had similar reducibility and excludes the formation of large amounts of cobalt (hydro)silicates. Due to the mild reaction conditions catalyst deactivation during reaction was not significant. Therefore, industrially relevant reaction conditions, i.e. pressures of 20 bar and high conversions should be applied to study the effect of the Co_3O_4 nanoparticle distribution on deactivation by sintering. Nevertheless, the observed comparable activities for catalysts with similar particle sizes, but various nanoparticle spacing qualify these materials to study a structure-performance relation for deactivation.

Table 4
Catalytic activity for the Fischer-Tropsch synthesis at 220 ºC and 1 bar of various catalysts prepared by solution impregnation (SI) and conventional drying (CD) or freeze-drying (FD) and calcination in different gas flows.

Catalyst preparation	Calcination atmosphere	reduction temperature (ºC)	CTY[a,b] (10^{-5} $mol_{CO}/g_{Co}/s$)	C_1[a,c] (wt%)	C_{5+}[a,c] (wt%)
Co_3O_4/SiO_2-SI-CD	N_2	450	3.70	19.9	51.5
Co_3O_4/SiO_2-SI-FD(LN_2/-45)	N_2	450	4.09	23.0	44.9
Co_3O_4/SiO_2-SI-CD	NO/N_2	550	5.20	20.9	49.9
Co_3O_4/SiO_2-SI-FD(LN_2/-45)	NO/N_2	550	6.20	23.3	44.0

[a] catalytic properties were determined after 20 hrs time-on-stream, [b] cobalt-time-yield, [c] selectivity.

4. Conclusions

The cobalt oxide nanoparticle distribution in Co/SiO_2 Fischer-Tropsch catalysts was successfully manipulated by varying the drying treatments. More specifically, this was achieved for a system with weak support-precursor interaction and at high metal loadings, using a commercially available silica-gel support and cobalt nitrate as precursor. Freeze-drying was applied to restrict precursor mobility during the drying step. Based on the different freezing point depressions of confined cobalt nitrate solution and cobalt nitrate hexahydrate salt, two freeze-drying methods were developed. DSC showed that by freezing at liquid nitrogen temperatures, both solution and salt solidified, while by freezing at -45 ºC only the confined cobalt nitrate salt crystallized. The Co_3O_4 distribution after decomposition of the nitrate largely represented the distribution of the precursor phase obtained by drying. Conventional drying led to the formation of clusters of individual nanoparticles, while freeze-drying starting at liquid nitrogen temperatures led to a uniform distribution of nanoparticles over the support. An egg-shell catalyst was obtained after solution impregnation and freeze-drying starting at -45 ºC, which is above the crystallization temperature of confined cobalt nitrate solution. An average particle size of 8 nm was obtained after calcination in a flow of N_2 and 4-6 nm particles were obtained by decomposition in 1% NO/N_2. All catalysts showed high activity for the Fischer-Tropsch reaction at 1 bar, showing similar reducibility of the oxides formed after the different drying treatments and calcination. The catalysts thus synthesized comprise an excellent platform to test the effect of nanoparticle spacing on deactivation by sintering under industrially relevant reaction conditions.

Acknowledgements

Mr. M. van Steenbergen (Utrecht University) is acknowledged for technical support and useful discussions on freeze-drying as well as thermal analysis. Dr. H. de Waard (University of Groningen) and Dr. Foppe Bakker (MSD) are acknowledged for providing access to freeze-drying equipment and sharing their expertise. Mw. E. van Donselaar (Utrecht University) is acknowledged for ultramicrotomy instructions. K.P.dJ., T.M.E and P.M. thank the Netherlands Organization for Scientific Research for funding (NWO TOP 700.57.341), P.E.dJ. thanks NWO-Vidi.

References

]1] C.H. Bartholomew, Appl. Catal.- A Gen. 212 (2001) 17-60.

]2] P. Forzatti, and L. Lietti, Catal. Today 52 (1999) 165-181.

]3] P.M. Arnal, M. Comotti, and F. Schuth, Angew. Chem., Int. Ed. 45 (2006) 8224-8227.

]4] S.H. Joo, J.Y. Park, C.K. Tsung, Y. Yamada, P.D. Yang, and G.A. Somorjai, Nat. Mater. 8 (2009) 126-131.

]5] W.F. Yan, S.M. Mahurin, Z.W. Pan, S.H. Overbury, and S. Dai, J. Am. Chem. Soc. 127 (2005) 10480-10481.

]6] L.Y. Li, D.L. King, J. Liu, Q.S. Huo, K.K. Zhu, C.M. Wang, M. Gerber, D. Stevens, and Y. Wang, Chem. Mater. 21 (2009) 5358-5364.

]7] A. Cao, and G. Veser, Nat. Mater. 9 (2010) 75-81.

]8] S.L. Soled, A. Malek, S. Miseo, J. Baumgartner, C. Kliewer, M. Afeworki, and P.A. Stevens, Scientific Bases for the Preparation of Heterogeneous

Catalysts, Proceedings of the 9th International Symposium 162 (2006) 103-110.
]9] A.M. Saib, D.J. Moodley, I.M. Ciobica, M.M. Hauman, B.H. Sigwebela, C.J. Weststrate, J.W. Niemantsverdriet, and J. van de Loosdrecht, Catal. Today 154 (2010) 271-282.
]10] A.V. Neimark, L.I. Kheifez, and V.B. Fenelonov, Ind. Eng. Chem. Prod. Res. Dev. 20 (1981) 439-450.
]11] E. Iglesia, S.L. Soled, J.E. Baumgartner, and S.C. Reyes, J. Catal. 153 (1995) 108-122.
]12] O. Borg, J.C. Walmsley, R. Dehghan, B.S. Tanem, E.A. Blekkan, S. Eri, E. Rytter, and A. Holmen, Catal. Lett. 126 (2008) 224-230.
]13] J.R.A. Sietsma, J.D. Meeldijk, J.P. den Breejen, M. Versluijs-Helder, A.J. van Dillen, P.E. de Jongh, and K.P. de Jong, Angew. Chem., Int. Ed. 46 (2007) 4547-4549.
]14] A. Martinez, C. Lopez, F. Marquez, and I. Diaz, J. Catal. 220 (2003) 486-499.
]15] J. van der Meer, I. Bardez, F. Bart, P.A. Albouy, G. Wallez, and A. Davidson, Micropor. Mesopor. Mat. 118 (2009) 183-188.
]16] I. Arslan, J.C. Walmsley, E. Rytter, E. Bergene, and P.A. Midgley, J. Am. Chem. Soc. 130 (2008) 5716-5719.
]17] E. Marceau, M. Che, J. Cejka, and A. Zukal, ChemCatChem 2 (2010) 413-422.
]18] A. Lekhal, B.J. Glasser, and J.G. Khinast, Chem. Eng. Sci. 56 (2001) 4473-4487.
]19] X. Liu, J.G. Khinast, and B.J. Glasser, Ind. Eng. Chem. Res. 49 (2010) 2649-2657.
]20] M. Komiyama, R.P. Merrill, and H.F. Harnsberger, J. Catal. 63 (1980) 35-52.
]21] M. Che, Z.X. Cheng, and C. Louis, J. Am. Chem. Soc. 117 (1995) 2008-2018.
]22] W. Chu, L.N. Wang, P.A. Chernavskii, and A.Y. Khodakov, Angew. Chem., Int. Ed. 47 (2008) 5052-5055.
]23] A.J. van Dillen, R.J.A.M. Terorde, D.J. Lensveld, J.W. Geus, and K.P. de Jong, J. Catal. 216 (2003) 257-264.
]24] N.F. Zheng, and G.D. Stucky, J. Am. Chem. Soc. 128 (2006) 14278-14280.
]25] A. Reyes, R. Vega, R. Bustos, and C. Araneda, Dry. Technol. 26 (2008) 1272-1285.
]26] V. Kirmaci, H. Usta, and T. Menlik, Dry. Technol. 26 (2008) 1570-1576.
]27] G.H. Chen, and W. Wang, Dry. Technol. 25 (2007) 29-35.
]28] C.J. Chen, D.D. Han, C.F. Cai, and X. Tang, J. Control. Release 142 (2010) 299-311.
]29] W. Wang, Int. J. Pharm. 203 (2000) 1-60.
]30] D.C. Portner, R.G.K. Leuschner, and B.S. Murray, Cryobiology 54 (2007) 265-270.
]31] C. Schwab, R. Vogel, and M.G. Ganzle, Cryobiology 55 (2007) 108-114.
]32] L. Qian, and H. Zhang, J. Chem. Technol. Biotechnol. 86 (2010) 172-184.
]33] K. Kraiwattanawong, N. Sano, and H. Tamon, Carbon 49 (2011) 3404-3411.
]34] T. Vergunst, F. Kapteijn, and J.A. Moulijn, Appl. Catal.- A Gen. 213 (2001) 179-187.
]35] X.L. Xi, Z.R. Nie, Y.B. Jiang, X.Y. Xu, and T.Y. Zuo, Powder Technol. 191 (2009) 107-110.
]36] H.J. Kim, S.M. Choi, S.H. Nam, M.H. Seo, and W.B. Kim, Appl. Catal.- A Gen. 352 (2009) 145-151.

]37] X. Carrier, J.F. Lambert, S. Kuba, H. Knozinger, and M. Che, J. Mol. Struct. 656 (2003) 231-238.
]38] J.D. Mellor, Fundamentals of freeze-drying. Academic Press, London New York San Fransisco, 1978.
]39] E.W. Flosdorf, Freeze-drying. Drying by sublimation. Reinhold Publishing corporation, New York, 1949.
]40] X.L. Tang, and M.J. Pikal, Pharm. Res. 21 (2004) 191-200.
]41] J.C. Kasper, and W. Friess, Eur. J. Pharm. Biopharm. 78 (2011) 248-263.
]42] J. Beirowski, S. Inghelbrecht, A. Arien, and H. Gieseler, J. Pharm. Sci. 100 (2011) 1958-1968.
]43] J.A. Searles, J.F. Carpenter, and T.W. Randolph, J. Pharm. Sci. 90 (2001) 872-887.
]44] B.G. Malmstrom, Exp. Cell Res. 2 (1951) 688-692.
]45] K.H. Gan, R. Bruttini, O.K. Crosser, and A.I. Liapis, Dry. Technol. 22 (2004) 1539-1575.
]46] M.J. Pikal, S. Shah, M.L. Roy, and R. Putman, Int. J. Pharm. 60 (1990) 203-217.
]47] M. Wolters, I.C.A. Contreras Andrade, P. Munnik, J.H. Bitter, P.E. de Jongh, and K.P. de Jong, Stud. Surf. Sci. Catal. 175 (2010) 69-76.
]48] T.M. Eggenhuisen, J.P. den Breejen, D. Verdoes, P.E. de Jongh, and K.P. de Jong, J. Am. Chem. Soc. 132 (2010) 18318-18325.
]49] J. Vakros, K. Bourikas, S. Perlepes, C. Kordulis, and A. Lycourghiotis, Langmuir 20 (2004) 10542-10550.
]50] J.R.A. Sietsma, H. Friedrich, A. Broersma, M. Versluijs-Helder, A.J. van Dillen, P.E. de Jongh, and K.P. de Jong, J. Catal. 260 (2008) 227-235.
]51] M. Wolters, P. Munnik, J.H. Bitter, P.E. de Jongh, and K.P. de Jong, J. Phys. Chem. C 115 (2011) 3332-3339.
]52] H. Friedrich, J.R.A. Sietsma, P.E. de Jongh, A.J. Verkleij, and K.P. de Jong, J. Am. Chem. Soc. 129 (2007) 10249-10254.
]53] P. Munnik, M. Wolters, A. Gabrielsson, S.D. Pollington, G. Headdock, J.H. Bitter, P.E. de Jongh, and K.P. de Jong, J. Phys. Chem. C 115 (2011) 14698-14706.
]54] G. Jacobs, T.K. Das, Y.Q. Zhang, J.L. Li, G. Racoillet, and B.H. Davis, Appl. Catal.- A Gen. 233 (2002) 263-281.
]55] J.P. den Breejen, J.R.A. Sietsma, H. Friedrich, J.H. Bitter, and K.P. de Jong, J. Catal. 270 (2010) 146-152.
]56] J.P. den Breejen, P.B. Radstake, G.L. Bezemer, J.H. Bitter, V. Froseth, A. Holmen, and K.P. de Jong, J. Am. Chem. Soc. 131 (2009) 7197-7203.